FULLY COMPRESSIBLE LARGE-EDDY SIMULATION OF WALL-JET TURBULENT MIXING: IMPROVED BOUNDARY CONDITIONS FOR EDGE, CORNER AND TRANSVERSE FLUXES.

Guido Lodato, Pascale Domingo and Luc Vervisch
INSA - Rouen, UMR-CNRS-6614-CORIA,
Campus du Madrillet, Avenue de l'Université, BP 8
76801 Saint Etienne du Rouvray Cedex, France
lodato@coria.fr, domingo@coria.fr, vervisch@coria.fr

ABSTRACT

Fully compressible Large-Eddy Simulation (LES) of high Reynolds impinging round-jet is performed in order to assess the impact of both inlet profiles and boundary conditions on turbulence development. The modification to the Navier-Stokes Characteristic Boundary Conditions (NSCBC) proposed by Yoo et al. (2005) is extended to the 3D problem and a specific treatment for the computational domain edges and corners is proposed together with compatibility conditions for inlet/outlet and wall/outlet joining regions. Comparisons of the statistical results against the experimental data demonstrate the effectiveness of the proposed improvement, which allows for reproducing mean flow velocity up to the computational domain limits.

INTRODUCTION

Impinging jets are of great interest for many practical applications in engineering and a better description of various phenomena characterizing such flow is still needed, as scalar mixing and heat exchange at the wall, turbulent mixing in the very near wall-jet region, etc. The high complexity of the flow field characterizing this configuration, makes the impinging jet a particularly difficult test bench for turbulence modeling. The flow is characterized by three main regions: (a) free jet, (b) stagnation-point and (c) wall-jet. Each of these regions retains a number of interesting features peculiar of this configuration (e.g. the influence of the jet's length scales in the near-wall region, the turbulent energy creation mechanism or the impact of the strong curvature on flow structure). Furthermore, the presence of the wall boundary layer and the relevant necessary grid refinement put some limitation to the use of LES.

Wall-jet interaction was studied by Hällqvist (2006) using low-Mach number LES without explicit Sub-Grid Scale (SGS) modeling. Compressible LES have been performed by Hadžiabdić and Hanjalić (2006) using an unstructured finite-volume code. In both cases, the computational grid was highly refined (5.5M nodes and 9.9M nodes respectively) leading to very well resolved simulations with an inlet forcing imposed by means of a precursor simulation of fully developed turbulent pipe flow.

We report on the assessment of the inlet/outlet boundary conditions when performing compressible LES of unexcited impinging round-jet with explicit SGS modeling starting from an assumed a priori simplified velocity profile. A specific treatment is discussed to deal with edges and corners when imposing boundary conditions in fully compressible simulations.

FLOW CONFIGURATION AND NUMERICS

LES have been performed by means of a parallel solver based on an explicit finite volume 4^{th} order centered skew-symmetric-like scheme by Ducros et al. (2000). The scheme is augmented by a blend of 2^{nd} and 4^{th} order artificial dissipation for spatial discretization (Tatsumi et al., 1995; Swanson and Turkel, 1992), in order to suppress spurious oscillations and damp high-frequency modes. A two-stage Runge-Kutta scheme is retained for time integration. Within the framework of LES approach, the Navier-Stokes equations are filtered with a low-pass filter, the low frequency components of the flow field—those which represent the large scale structures of the flow—being directly resolved, and the coupling term arising from the non-linear convective term being modeled by the Sub-Grid Scale model. We adopt an implicit filtering approach, therefore the filter's cutoff length Δ is equal to the local grid spacing, while SGS terms are modeled using the eddy viscosity assumption of the Wall-Adapting Local Eddy-viscosity model proposed by Nicoud and Ducros (1999) in order to have a better scaling of the eddy viscosity in the near-wall region.

The configuration has been chosen to have a direct reference with experimental data produced by Cooper et al. (1993). Therefore, the jet nozzle is located at a distance equal to twice the jet diameter D from the impingement wall and the Reynolds number, based on the jet diameter and the bulk velocity U_b, is equal to 23,000. The computational domain is a cartesian grid with the x-axis aligned with the axis of the jet. Three meshes have been used depending on the test performed: a 170k ($45 \times 62 \times 62$ for a physical domain of $2D \times 6D \times 6D$) mesh points domain for the qualitative assessment of the boundary conditions, a 1.5M ($70 \times 146 \times 146$ for a physical domain of $2D \times 7D \times 7D$) mesh points domain for accurate comparison with experimental data and a 4.1M ($70 \times 242 \times 242$ for a physical domain of $2D \times 14D \times 14D$) mesh points extended domain to assess the influence of the domain width.

To avoid problems arising from the influence of the boundary condition over the flow, it is generally advisable to have the boundaries quite far from the jet axis. Still, the pressure waves developing especially during the initial transient, can negatively affect the solution due to unphysical wave reflections at the frontiers of the computational domain. In order to limit both of these effects, all the boundary conditions are enforced using a modified version of the NSCBC strategy (Poinsot and Lele, 1992): no-slip adiabatic wall condition for the impingement wall, subsonic non-reflecting outflow for the four lateral sides and subsonic non-reflecting inflow with relaxed velocities and tempera-

ture (Yoo et al., 2005). Furthermore, a correlated random noise (Klein et al., 2003) is injected at the inlet with a time-step independent sampling rate computed from the jet's characteristic time-scale.

MODIFIED NSCBC BOUNDARY CONDITIONS

The NS Equations are rewritten in terms of the characteristic wave's amplitude time variation $\mathscr{L}_i$ by means of the characteristic analysis (Thompson, 1990). Supposing that the boundary is normal to x_1 and choosing $\mathbf{U} = \begin{vmatrix} \rho & u_1 & u_2 & u_3 & p \end{vmatrix}^T$ as the primitive variables vector, the system becomes:

$$\frac{\partial \rho}{\partial t} + d_1 + \frac{\partial}{\partial x_t}(m_t) = 0 \tag{1}$$

$$\frac{\partial m_1}{\partial t} + u_1 d_1 + \rho d_2 + \frac{\partial}{\partial x_t}(m_1 u_t) = \frac{\partial \tau_{1j}}{\partial x_j} \tag{2}$$

$$\frac{\partial m_2}{\partial t} + u_2 d_1 + \rho d_3 + \frac{\partial}{\partial x_t}(m_2 u_t) + \frac{\partial p}{\partial x_2} = \frac{\partial \tau_{2j}}{\partial x_j} \tag{3}$$

$$\frac{\partial m_3}{\partial t} + u_3 d_1 + \rho d_4 + \frac{\partial}{\partial x_t}(m_3 u_t) + \frac{\partial p}{\partial x_3} = \frac{\partial \tau_{3j}}{\partial x_j} \tag{4}$$

$$\frac{\partial \rho E}{\partial t} + \frac{1}{2} u_k u_k d_1 + \frac{d_5}{\gamma - 1} + m_k d_{k+1} + \frac{\partial}{\partial x_t}\left[(\rho E + p)\, u_t\right] = \frac{\partial (u_j \tau_{ij})}{\partial x_i} - \frac{\partial q_i}{\partial x_i} \tag{5}$$

where $k = 1, 2, 3$ and the subscript t indicates derivation in the directions parallel to the boundary—in this case $t = 2, 3$—and the d_i terms are known functions of the wave amplitude time variations $\mathscr{L}_i$:

$$\mathbf{d} = \begin{pmatrix} \frac{1}{c^2}\left[\mathscr{L}_2 + \frac{1}{2}(\mathscr{L}_5 + \mathscr{L}_1)\right] \\ \frac{1}{2\rho c}(\mathscr{L}_5 - \mathscr{L}_1) \\ \mathscr{L}_3 \\ \mathscr{L}_4 \\ \frac{1}{2}(\mathscr{L}_5 + \mathscr{L}_1) \end{pmatrix} \tag{6}$$

In the framework of the standard NSCBC approach, all the incoming wave amplitudes $\mathcal{L}_i$ are imposed under the hypothesis that the flow at the boundary can be regarded as *Locally Mono-Dimensional and Inviscid*. The so called LODI system, which is used to enforce the boundary conditions, is in fact built from the Navier-Stokes equations for primitive variables written in characteristic form and putting to zero all the transverse convective terms and pressure gradients terms, as well as all the diffusive terms:

$$\begin{cases} \dfrac{\partial \rho}{\partial t} + \dfrac{1}{c^2}\left[\mathscr{L}_2 + \dfrac{1}{2}(\mathscr{L}_5 + \mathscr{L}_1)\right] = 0 \\ \dfrac{\partial u_1}{\partial t} + \dfrac{1}{2\rho c}(\mathscr{L}_5 - \mathscr{L}_1) = 0 \\ \dfrac{\partial u_2}{\partial t} + \mathscr{L}_3 = 0 \\ \dfrac{\partial u_3}{\partial t} + \mathscr{L}_4 = 0 \\ \dfrac{\partial p}{\partial t} + \dfrac{1}{2}(\mathscr{L}_5 + \mathscr{L}_1) = 0 \end{cases} \tag{7}$$

The problem under study is characterized by a strong tridimensionalty of the flow field at the boundary. The LODI assumption has proven to be too restrictive to reduce boundary reflection to an acceptable level and to limit unphysical flow distortion, especially in regions where the flow is not aligned in the direction normal to the boundary. Furthermore, the relaxed quantities are not able to reach their target value in regions where the flow is characterized by strong convection in the boundary plane, leading to non-negligible transverse terms. Better results can be achieved including these transverse terms in the computation of incoming wave amplitudes, as already pointed out by Yoo et al. (2005) for two-dimentional counterflow flames simulation. The LODI system is therefore augmented with the contribution of transverse convection[1]:

$$\begin{cases} \dfrac{\partial \rho}{\partial t} + \dfrac{1}{c^2}\left[\mathscr{L}_2 + \dfrac{1}{2}(\mathscr{L}_5 + \mathscr{L}_1)\right] - \mathscr{T}_1 = 0 \\ \dfrac{\partial u_1}{\partial t} + \dfrac{1}{2\rho c}(\mathscr{L}_5 - \mathscr{L}_1) - \mathscr{T}_2 = 0 \\ \dfrac{\partial u_2}{\partial t} + \mathscr{L}_3 - \mathscr{T}_3 = 0 \\ \dfrac{\partial u_3}{\partial t} + \mathscr{L}_4 - \mathscr{T}_4 = 0 \\ \dfrac{\partial p}{\partial t} + \dfrac{1}{2}(\mathscr{L}_5 + \mathscr{L}_1) - \mathscr{T}_5 = 0 \end{cases} \tag{8}$$

with

$$\boldsymbol{\mathcal{T}} = \begin{pmatrix} -\frac{\partial}{\partial x_t}(\rho u_t) \\ -u_t \frac{\partial}{\partial x_t}(u_1) \\ -u_t \frac{\partial}{\partial x_t}(u_2) - \frac{1}{\rho}\frac{\partial p}{\partial x_2} \\ -u_t \frac{\partial}{\partial x_t}(u_3) - \frac{1}{\rho}\frac{\partial p}{\partial x_3} \\ -u_t \frac{\partial p}{\partial x_t} - \gamma p \frac{\partial}{\partial x_t}(u_t) \end{pmatrix} \qquad (t = 2, 3) \tag{9}$$

It should be noted that system (8), which is used to compute incoming waves, refers to the *outside* flow field. $\mathscr{T}_i$ terms, therefore, should, in principle, be computed on the external flow. This consideration poses a limit on the use of transverse terms since the external flow field is, in general, not known *a priori*. The most immediate approach would be to approximate $\mathscr{T}_i$ using the computed internal solution. This technique, indeed, works perfectly for the inflow boundary condition, where the convergence of the solution toward the target values is definitely improved (see figure 1, top). Nonetheless, for the outflow boundary, even though the convergence toward the target pressure become faster and more accurate (see figure 1, bottom), the flow field shows a tendency to align in the transverse direction and the solution, eventually, becomes unstable. As suggested by Yoo et al. (2005), a remedy for this problem is to add a small relaxation to the transverse terms toward a reasonable exact known solution. In the present case, relaxation toward the inviscid potential solution for the *Axisymmetric Stagnation-Point Flow* (Schlichting and Gersten, 2000) has proven to be effective to ensure stability. From a qualitative point of view, the inclusion of transverse terms in the computation of incoming wave amplitude variations shows a dramatic impact in reducing flow deformation at the boundary, especially when the flow itself is characterized by a strong tridimensionality. Figure 2 shows a comparison of the behavior of the modified boundary conditions when the big toroidal vortex, which develops at the beginning of the injection, meets the outflow boundaries.

Modified Subsonic Non-Reflecting Outflow. The outflow condition must be imposed to obtain $\mathscr{L}_1$, with $\mathscr{T}_i$ terms

[1] More precisely, transverse convection and pressure gradients. In order to avoid confusion, they will be called transverse terms in what follows to imply that pressure gradients are also included

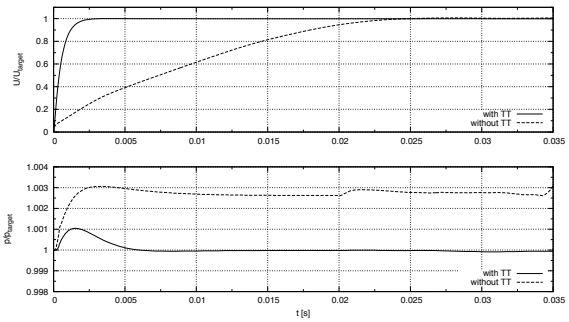

Figure 1: Transverse terms influence on boundary accuracy. Time evolution of the normalized computed inlet velocity (top) and outlet pressure (bottom). Solid-line: with transverse terms. Dash-line: without transverse terms.

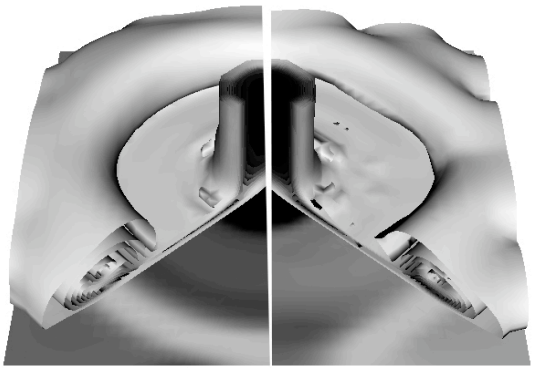

Figure 2: Transverse Terms influence on flow distortion. Isosurfaces of velocity field in the early stages of the simulation with transverse terms (left) and without transverse terms (right).

being computed from interior points; nonetheless, as previously mentioned, it's advisable to impose a small relaxation for transverse terms. If the boundary is located at $x_1 = L_x$ ($\mathscr{L}_1$ is the only incoming term), the relevant condition reads:

$$\left(\frac{\partial p}{\partial t} - \rho c \frac{\partial u_1}{\partial t}\right) + \alpha\,(p - p_\infty) - \beta\,(\mathscr{T}_5 - \rho c \mathscr{T}_2 - \mathscr{T}_{ex}) = 0 \tag{10}$$

where α is the relaxation parameter for the pressure, $\beta \in [0\colon 1]$ is the relaxation parameter for the transverse terms and $\mathscr{T}_{ex}$ represents the exact transverse terms for the $\mathscr{L}_1$ equation, namely:

$$\mathscr{T}_{ex} = -\left[u_{0t}\frac{\partial p_0}{\partial x_t} + \gamma p_0 \frac{\partial u_{0t}}{\partial x_t} - \rho_0 c_0 u_{0t}\frac{\partial u_{01}}{\partial x_t}\right] \tag{11}$$

the subscript 0 indicating quantities referring to the chosen exact solution (i.e. Axisymmetric Stagnation-Point Flow). From the system 8, the equation for $\mathscr{L}_1$ then becomes:

$$\mathscr{L}_1 = \alpha\,(p - p_\infty) + (1-\beta)\,(\mathscr{T}_5 - \rho c \mathscr{T}_2) + \beta \mathscr{T}_{ex} \tag{12}$$

Modified Non-Reflecting Inflow. The steady state pressure field is generally not known a priori, therefore the direct imposition of the target velocity can lead to strong initial pressure waves and unphysical oscillations. Due to the high value of the target velocity for the problem under study, negative pressure regions developed, in the nozzle area, just beneath these strong initial pressure waves. In order to avoid this problem, the target velocity and temperature are relaxed towards the target values, rather than being imposed directly (Yoo et al., 2005); therefore, the solution is able to reach the steady state in a smoother way and, at the same time, pressure waves reflected back by the impingement wall leave the domain trough the inlet with negligible reflection. Supposing that the $\mathscr{L}_1$ is the only outgoing wave ($x_1 = 0$), the nonreflecting subsonic inflow condition is:

$$\begin{cases} \left(\dfrac{\partial p}{\partial t} + \rho c \dfrac{\partial u_1}{\partial t}\right) + \beta_5(u_1 - u_{1_0}) &= 0 \\ \dfrac{\partial}{\partial t}\left(\dfrac{p}{\rho^\gamma}\right) + \beta_2(T - T_0) &= 0 \\ \dfrac{\partial u_2}{\partial t} + \beta_3(u_2 - u_{2_0}) &= 0 \\ \dfrac{\partial u_3}{\partial t} + \beta_4(u_3 - u_{3_0}) &= 0 \end{cases} \tag{13}$$

where the $\beta_2, \ldots, \beta_5$ are the relaxation parameters for the relevant quantities and u_{1_0}, u_{2_0}, u_{3_0} and T_0 are the target values for velocities and temperature. As before, the system 8 is used to obtain the unknown wave amplitude variations:

$$\mathscr{L}_5 = \beta_5(u_1 - u_{1_0}) + \mathscr{T}_5 + \rho c \mathscr{T}_2 - \rho\, c\, \frac{\mathrm{d}U_0}{\mathrm{d}t} \tag{14}$$

$$\mathscr{L}_2 = \beta_2(T - T_0) + c^2 \mathscr{T}_1 - \mathscr{T}_5 \tag{15}$$

$$\mathscr{L}_3 = \beta_3(u_2 - u_{2_0}) + \mathscr{T}_3 - \frac{\mathrm{d}V_0}{\mathrm{d}t} \tag{16}$$

$$\mathscr{L}_4 = \beta_4(u_3 - u_{3_0}) + \mathscr{T}_4 - \frac{\mathrm{d}W_0}{\mathrm{d}t} \tag{17}$$

U_0, V_0 and W_0 are additional signals which can be superimposed on the target solution by mean of their time derivative. In particular, they have been used to inject the correlated random noise.

Treatment of Edges and Corners

On the edges of the computational domain, two sets of waves are traveling along orthogonal directions and two main questions are posed: (a) it may be needed to impose two types of boundary conditions at the same location (wall-inflow, wall-outlet or inflow-outlet) and, in general, compatibility conditions have to be used in order to ensure well posedness; (b) normal terms for one boundary become transverse terms for the other and *vice versa*, therefore, transverse terms' implementation has to be adapted at this specific grid location. In other words, as pointed out by Valorani and Favini (1998), unknown incoming waves become coupled on edges and corners. The Navier-Stokes equations have now to be written in characteristic form considering two directions. Supposing the case of boundaries normal to x_1 and x_2 (the edge is along x_3), new $\mathscr{M}_i$ terms appear relevant to waves traveling along x_2 and the system 8 becomes[2]:

$$\begin{cases} \dfrac{\partial \rho}{\partial t} + \dfrac{1}{c^2}\left[\mathscr{L}_2 + \dfrac{1}{2}(\mathscr{L}_5 + \mathscr{L}_1)\right] \\ \qquad + \dfrac{1}{c^2}\left[\mathscr{M}_3 + \dfrac{1}{2}(\mathscr{M}_5 + \mathscr{M}_1)\right] - \mathscr{T}_1 = 0 \\ \dfrac{\partial u_1}{\partial t} + \dfrac{1}{2\rho c}(\mathscr{L}_5 - \mathscr{L}_1) + \mathscr{M}_2 - \mathscr{T}_2 = 0 \\ \dfrac{\partial u_2}{\partial t} + \mathscr{L}_3 + \dfrac{1}{2\rho c}(\mathscr{M}_5 - \mathscr{M}_1) - \mathscr{T}_3 = 0 \\ \dfrac{\partial u_3}{\partial t} + \mathscr{L}_4 + \mathscr{M}_4 - \mathscr{T}_4 = 0 \\ \dfrac{\partial p}{\partial t} + \dfrac{1}{2}(\mathscr{L}_5 + \mathscr{L}_1) + \dfrac{1}{2}(\mathscr{M}_5 + \mathscr{M}_1) - \mathscr{T}_5 = 0 \end{cases} \tag{18}$$

[2]The extension to the case of domain corners is straightforward and is done expressing convection and pressure gradient along x_3 in terms of wave amplitude variations $\mathscr{N}_i$.

The $\mathscr{T}_i$ terms represent convection and pressure gradient along x_3 only. Depending on the kind of boundary conditions to be imposed a linear system of equations in the incoming unknown waves amplitudes is solved as given below, while the compatibility conditions, if necessary, are imposed in terms of constraints on the solution.

Outflow/Outflow with Transverse Terms Relaxation. System 18, in analogy with system 8, can be used to derive boundary conditions for unknown incoming waves. Once the two boundary types are identified, a set of n conditions involving time derivatives of primitive variables is imposed which corresponds, through system 18, to a set of n equations in $\mathscr{L}_i$ and $\mathscr{M}_i$, the number of unknown wave amplitude variations being exactly n. Supposing, for instance, that the edge is the joining region between two outflows located at $x_2 = L_y$ and $x_3 = L_z$ ($\mathscr{L}_1$, $\mathscr{M}_1$ unknown), boundary conditions are:

$$\begin{cases} \left(\dfrac{\partial p}{\partial t} - \rho c \dfrac{\partial u_1}{\partial t}\right) + \alpha\,(p - p_\infty) - \beta\left(\mathbb{T}^1 - \mathscr{T}^1_{ex}\right) = 0 \\ \left(\dfrac{\partial p}{\partial t} - \rho c \dfrac{\partial u_2}{\partial t}\right) + \alpha\,(p - p_\infty) - \beta\left(\mathbb{T}^2 - \mathscr{T}^2_{ex}\right) = 0 \end{cases} \tag{19}$$

where $\mathscr{T}^1_{ex}$ and $\mathscr{T}^2_{ex}$—which refer to the $\mathscr{L}_1$ and $\mathscr{M}_1$ equations respectively—are computed on the supposed exact solution. $\mathbb{T}^1$ and $\mathbb{T}^2$ are the analogous terms relevant to the computed solution and can be explicitly identified resorting to the system 8:

$$\left(\frac{\partial p}{\partial t} - \rho c \frac{\partial u_1}{\partial t}\right) + \mathscr{L}_1 + \underbrace{\frac{1}{2}\left(\mathscr{M}_5 + \mathscr{M}_1\right) - \rho c \mathscr{M}_2 - \left(\mathscr{T}_5 - \rho c \mathscr{T}_2\right)}_{-\mathbb{T}^1} = 0 \tag{20}$$

$$\left(\frac{\partial p}{\partial t} - \rho c \frac{\partial u_2}{\partial t}\right) + \mathscr{M}_1 + \underbrace{\frac{1}{2}\left(\mathscr{L}_5 + \mathscr{L}_1\right) - \rho c \mathscr{L}_3 - \left(\mathscr{T}_5 - \rho c \mathscr{T}_3\right)}_{-\mathbb{T}^2} = 0 \tag{21}$$

From the system 19 and the equations 20 and 21, the solving system for $\mathscr{L}_1$ and $\mathscr{M}_1$ becomes:

$$\begin{cases} \mathscr{L}_1 + \dfrac{1-\beta}{2}\mathscr{M}_1 = \alpha\,(p - p_\infty) + (1-\beta)\widetilde{\mathbb{T}}^1 + \beta\mathscr{T}^1_{ex} \\ \dfrac{1-\beta}{2}\mathscr{L}_1 + \mathscr{M}_1 = \alpha\,(p - p_\infty) + (1-\beta)\widetilde{\mathbb{T}}^2 + \beta\mathscr{T}^2_{ex} \end{cases} \tag{22}$$

$\widetilde{\mathbb{T}}^1$ and $\widetilde{\mathbb{T}}^2$ being the known part of transverse terms:

$$\widetilde{\mathbb{T}}^1 = -\frac{1}{2}\mathscr{M}_5 + \rho c \mathscr{M}_2 + \left(\mathscr{T}_5 - \rho c \mathscr{T}_2\right) \tag{23}$$

$$\widetilde{\mathbb{T}}^2 = -\frac{1}{2}\mathscr{L}_5 + \rho c \mathscr{M}_3 + \left(\mathscr{T}_5 - \rho c \mathscr{T}_3\right) \tag{24}$$

It should be noted that, being $0 \le \beta \le 1$, the system 22 always admits solution[3]; nonetheless, some care has to be taken in general as, depending on the particular boundaries considered, a check on this regard is recommended. On the other hand, when no relaxation of transverse terms is necessary, the matrix of coefficient will be fixed, as can be verified setting $\beta = 0$ in system 22.

[3]The determinant of the relevant matrix of coefficient is zero for $\beta = -1$ and $\beta = 3$

Outflow/Wall Compatibility Condition. On this kind of edge, in principle, one should impose the pressure, for what concerns the outlet condition, and velocity, for what concern the wall condition. As suggested by Poinsot and Lele (1992), just imposing all these quantities at the same time simply does not work, but allowing smooth transient for the pressure, namely relaxing outlet pressure, is a possible solution, and indeed it does work. Since the velocity at the wall is zero, the only non-zero wave amplitude variations are $\mathscr{L}_{1,5}$ and $\mathscr{M}_{1,5}$ (those characterized by characteristic speeds $u_1 \pm c$ and $u_2 \pm c$). $\mathscr{T}_1$, $\mathscr{T}_2$, $\mathscr{T}_3$ and $\mathscr{T}_5$ are zero as well. Supposing the wall is normal to x_1 and the edge is located at $x_1 = L_x$ and $x_2 = 0$, the boundary conditions are imposed by setting to zero the time derivative of u_1 and by the pressure relaxation condition (second equation in system 19, in the present case with the + sign for the ρc term). From system 18 the relevant equations are:

$$\frac{\partial u_1}{\partial t} + \frac{1}{2\rho c}\left(\mathscr{L}_5 - \mathscr{L}_1\right) = 0 \tag{25}$$

$$\left(\frac{\partial p}{\partial t} + \rho c \frac{\partial u_2}{\partial t}\right) + \mathscr{M}_5 + \underbrace{\frac{1}{2}\left(\mathscr{L}_5 + \mathscr{L}_1\right)}_{-\mathbb{T}^2} = 0 \tag{26}$$

and the solving system for $\mathscr{L}_1$ and $\mathscr{M}_5$ reads:

$$\begin{cases} \mathscr{L}_1 = \mathscr{L}_5 \qquad [\Rightarrow \mathbb{T}^2 = -\mathscr{L}_5] \\ \mathscr{M}_5 = \alpha\,(p - p_\infty) + (1-\beta)\mathbb{T}^2 + \beta\mathscr{T}^2_{ex} \end{cases} \tag{27}$$

u_2 and u_3 are simply forced to zero.

Inlet/Outflow Compatibility Condition. Although a bit more cumbersome (there are 5 unknowns in this case), the very same procedure used to build the outflow/outflow condition could be followed. Inlet and outlet boundary conditions could be simultaneously imposed. Even allowing smooth transients for pressure, the two boundary conditions have shown problems of stability when simultaneously imposed. A simple remedy, which has proven effective, is to set to zero the incoming wave amplitude relevant to the outflow boundary ("perfectly non-reflecting" outflow). In this way, the pressure is left free to adapt to the local flow field and tends anyway to the expected value due to the effect of the neighboring regions. Supposing for instance the inlet normal to x_1 and located at $x_1 = 0$ and the outflow located at $x_2 = L_y$, imposing the inlet boundary condition (system 13) through the system 18, leads to the expression for the unknown wave amplitude variations:

$$\begin{cases} \mathscr{M}_1 = 0 \qquad \text{(compatibility condition)} \\ \mathscr{L}_5 = \beta_5(u_1 - u_{1_0}) - \dfrac{1}{2}\mathscr{M}_5 + \mathscr{T}_5 + \rho c\,(\mathscr{T}_2 - \mathscr{M}_2) - \rho\, c\, \dfrac{\mathrm{d}U_0}{\mathrm{d}t} \\ \mathscr{L}_2 = \beta_2(T - T_0) - \mathscr{M}_3 + c^2\mathscr{T}_1 - \mathscr{T}_5 \\ \mathscr{L}_3 = \beta_3(u_2 - u_{2_0}) - \dfrac{1}{2\rho c}\mathscr{M}_5 + \mathscr{T}_3 - \dfrac{\mathrm{d}V_0}{\mathrm{d}t} \\ \mathscr{L}_4 = \beta_4(u_3 - u_{3_0}) - \mathscr{M}_4 + \mathscr{T}_4 - \dfrac{\mathrm{d}W_0}{\mathrm{d}t} \end{cases} \tag{28}$$

INLET PROFILE INFLUENCE

The influence of the target velocity profile has been assessed using three profiles:

- Top Hat profile.

$$\frac{U(r)}{U_{cl}} = \begin{cases} 1 & \text{if } 0 \le 2r/D \le 1, \\ 0 & \text{if } 2r/D > 1. \end{cases} \tag{29}$$

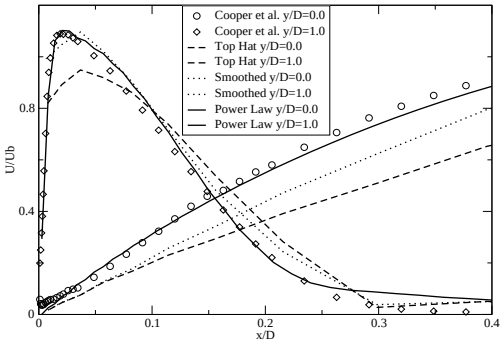

Figure 3: Inlet profile shape influence. Mean streamwise velocity. Symbols: experimental data. Lines: power law profile ($n = 7.4$, Eq. 31). Dots: Smoothed profile ($D/\theta = 20$, Eq. 30). Dashed lines: top hat profile (Eq. 29).

- Smoothed profile (Lesieur et al., 2005):

$$\frac{U(r)}{U_{cl}} = \frac{1}{2}\left[1 - \tanh\left(\frac{1}{8}\frac{D}{\theta}\left(\frac{2r}{D} - \frac{D}{2r}\right)\right)\right] \qquad (30)$$

- Power Law profile for turbulent pipe flow:

$$\frac{U(r)}{U_{cl}} = \left(1 - \frac{2r}{D}\right)^{1/n} \qquad (31)$$

where U_{cl} is the centerline velocity, r is the distance from the jet axis, θ is a parameter to control the shear layer thickness and n is a coefficient which depends on the pipe's friction factor[4].

In figure 3, a comparison for these different inlet profiles is displayed. The shape of the profile used has a dramatic impact on the simulated flow. An almost top hat-shape profile is not effective in catching the experimental data: the spreading of the jet before the stagnation point is too high and the jet core does not retain enough kinetic energy. The axial velocity is also lower. Furthermore, the shear layer thickness is not well controlled and depends on the grid refinement. Smoothed profiles resembling a fully developed pipe flow give better results; the shear layer thickness can be used to fine tune the profile but still, it is not possible to retain enough kinetic energy on the centerline while maintaining the expected U_b/U_{cl} ratio. The best results have been obtained using the power law profile. The fairly good agreement with the experimental data (see also figure 5) clearly justify the use of this profile when a pre-simulation of a fully developed turbulent pipe flow cannot be performed, as it would be the case when simulating more complex systems.

DOMAIN WIDTH INFLUENCE

The results from two simulations made with different domain widths (7D and 14D) and using the smoothed inlet profile are shown in figure 4. Data have been sampled at fixed locations near the jet (y/D=0.0–1.0) and far from it (y/D=2.5–3.0); the latter sampling locations are, for the small domain case, just before the outflow. The presence of the outflow has a negligible effect on the average flow

[4]A value of $n = 7$ is generally used; in what follows, n has been set to 7.4 in order to retain the same ratio between bulk velocity and centerline velocity as in the Cooper's experiment.

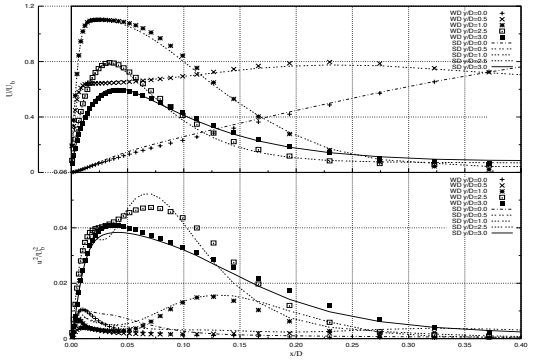

Figure 4: Domain size influence. Average streamwise (top) and fluctuation velocity (bottom). *Wide Domain* (symbols): outlet at $y/D = 7.0$, 4.1M mesh points. *Small Domain* (lines): outlet at $y/D = 3.5$, 1.5M mesh points.

field; the influence on the fluctuating parts is slightly more pronounced though, especially approaching the boundary, where the peak in the case of the small domain is around 10% higher. This suggests that the outlet boundary conditions, and its acoustic coupling with the inlet conditions, are only slightly perturbing the flow.

COMPARISON AGAINST EXPERIMENTS

Statistical results have been extracted on the 1.5M mesh points run for comparison with the experimental data. Averaging has been performed, after the establishment of a reasonably developed flow, over a time equal to about $61D/U_b$ seconds for a statistical sample of 3,400 data. Furthermore, assuming the validity of the Taylor hypothesis, additional averaging has been done around the jet's axis for a total sample ranging from 108,800 and 911,200 data depending on the distance of the sampling location from the axis. The simulation shows fairly good agreement in terms of mean velocity profiles at all the locations (see figure 5); average velocity is slightly overpredicted for $x/D > 0.025$ at almost all the locations, due probably to the approximation related to the inlet profile used, which is not able to fully resemble the developed turbulent pipe flow. Nonetheless, the boundary, which is located just after the last sampling location, does not have a strong impact, and the overall accuracy seems to be well preserved. Turbulent fluctuations are given in figure 6. Near the jet, turbulence development follows the expected behavior and the turbulent kinetic energy is fairly well predicted. On the other hand, in the wall-jet region, turbulent energy becomes higher than expected and this accounts for an excess in radial fluctuations in the near wall region and an excess in transverse fluctuations right above it. This level of fluctuations is sensitive to the inlet forcing and to the artificial dissipation that is added in the numerics, it is therefore expected that some slight adjustments would provide results very close to the measurements. Nevertheless, the novel boundary treatment discussed above allows for decoupling the fluctuating simulated flow from the imposed limits of the computational domain, as shown in figure 7 (middle), where coherent vortex structures are shown by means of isosurfaces of $Q = 0.5(\partial u_i/\partial x_j)(\partial u_j/\partial x_i)$. The typical size of vortical structures in the wall-jet region is about the same as in the jet shear layer, meaning that the information travels from the inlet without being perturbed by the outlets.

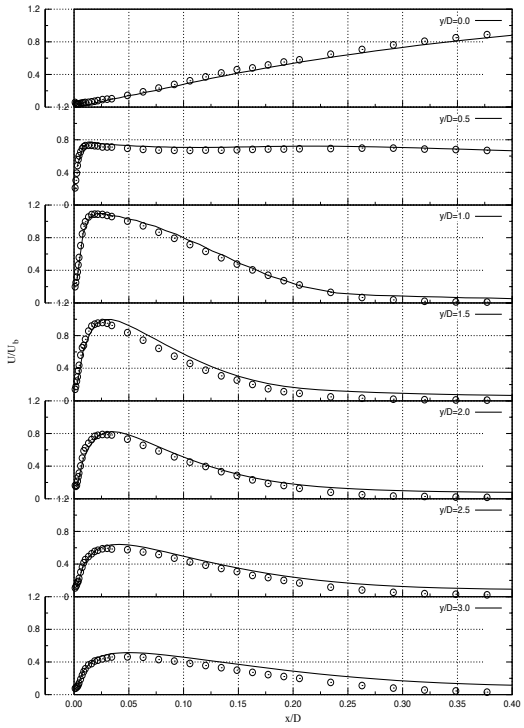

Figure 5: Normalized streamwise average velocity profiles. Symbol: Measurement. Line: LES.

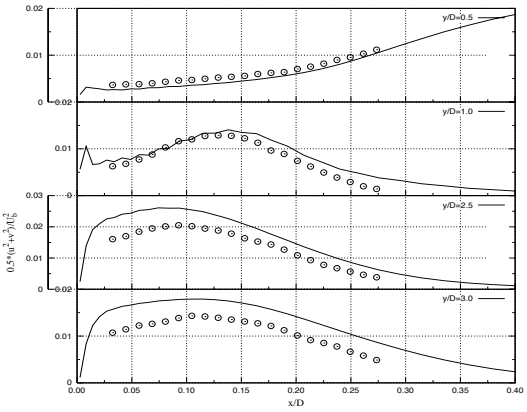

Figure 6: Normalized transverse velocity fluctuation profiles. Symbol: Measurement. Line: LES.

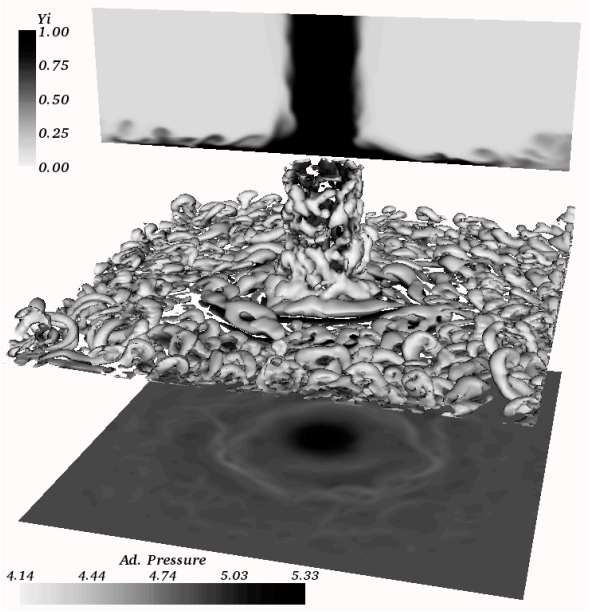

Figure 7: Flow visualization. Passive scalar radial distribution (top); $Q = 0.5U_b^2/D^2$ iso-surface (middle); Adimensionalized pressure $p/(\rho_0 U_b^2)$ wall distribution (bottom)

REFERENCES

Cooper, D., D. Jackson, B. Launder, and G. Liao, 1993. "Impinging jet studies for turbulence model assessment—I. flow-field experiments". *International Journal of Heat and Mass Transfer 36*(10), 2675–2684.

Ducros, F., F. Laporte, T. Soulères, V. Guinot, P. Moinat, and B. Caruelle, 2000. "High-order fluxes for conservative skew-symmetric-like schemes in structured meshes: Application to compressible flows". *Journal of Computational Physics 161*, 114–139.

Hadžiabdić, M. and K. Hanjalić, 2006. "LES of flow and heat transfer in a round impinging jet". In E. Lamballais, R. Friedrich, B. J. Geurts, and O. Métais (Eds.), *Direct and Large-Eddy Simulation VI*, Volume 10 of *ERCOFTAC Series*, pp. 477–486. Springer Netherlands.

Hällqvist, T., 2006, March. *Large Eddy Simulation of Impinging Jets with Heat Transfer*. Ph. D. thesis, Royal Institute of Technology, Department of Mechanics, S-100 44 Stockholm, Sweden.

Klein, M., A. Sadiki, and J. Janicka, 2003. "A digital filter based generation of inflow data for spatially developing direct numerical or large eddy simulations". *Journal of Computational Physics 186*, 652–665.

Lesieur, M., O. Métais, and P. Comte, 2005. *Large-Eddy Simulations of Turbulence*, Chapter 6, pp. 110. Cambridge University Press.

Nicoud, F. and F. Ducros, 1999, September. "Subgrid-scale stress modelling based on the square of the velocity gradient tensor". *Flow, Turbulence and Combustion 62*(3), 183–200.

Poinsot, T. and S. Lele, 1992. "Boundary conditions for direct simulations of compressible viscous flows". *Journal of Computational Physics 101*, 104–129.

Schlichting, H. and K. Gersten, 2000. *Boundary-Layer Theory* (8 ed.). Springer-Verlag Berlin Heidelberg.

Swanson, R. and E. Turkel, 1992. "On central-difference and upwind schemes". *Journal of Computational Physics 101*, 292–306.

Tatsumi, S., L. Martinelli, and A. Jameson, 1995, February. "Flux-limited schemes for the compressible navier-stokes equations". *AIAA Journal 33*(2), 252–261.

Thompson, K. W., 1990. "Time dependent boundary conditions for hyperbolic systems, II". *Journal of Computational Physics 89*, 439–461.

Valorani, M. and B. Favini, 1998, November. "On the numerical integration of multi-dimensional, initial boundary value problems for the euler equations in quasi-linear form". *Numerical Methods for Partial Differential Equations 14*(6), 781–814.

Yoo, C., Y. Wang, A. Trouvé, and H. Im, 2005, November. "Characteristic boundary conditions for direct simulations of turbulent counterflow flames". *Combustion Theory and Modeling 9*(4), 617–646.